Organic & Biomolecular Chemistry

Accepted Manuscript

ROYAL SOCIETY OF CHEMISTRY

www.rsc.org/obc

QSAR Study on the Inhibition Mechanism of Matrix Metalloproteinase-12 by Arylsulfone Analogs Based on Molecular Orbital Calculations

Seiji Hitaoka,[a] Hiroshi Chuman,[b,*] and Kazunari Yoshizawa[a,*]

[a]Institute for Materials Chemistry and Engineering and International Research Center for Molecular System, Kyushu University, Fukuoka 819-0395, Japan

[b]Institute of Health Biosciences, The University of Tokushima Graduate School, 1-78 Shomachi, Tokushima 770-8505, Japan

Corresponding Authors:

Hiroshi Chuman (H.C), Ph.D. and Kazunari Yoshizawa (K.Y.), Ph.D.

*H.C.: E-mail: hchuman@tokushima-u.ac.jp. Tel.: +81-88-633-7257. Fax: +81-88-633-9508.

*K.Y.: E-mail: kazunari@ms.ifoc.kyushu-u.ac.jp. Tel.: +81-92-802-2529. Fax: +81-92-802-2528.

Table of contents entry: *The inhibition mechanism of matrix metalloproteinase-12 by arylsulfone analogs is revealed by a comprehensive computational approach including docking simulations, molecular orbital calculations, and QSAR.*

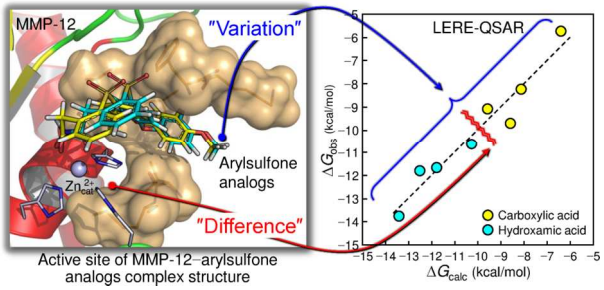

Abstract

A binding mechanism between human matrix metalloproteinase-12 (MMP-12) and eight arylsulfone analogs having two types of carboxylic and hydroxamic acids as the most representative zinc binding group is investigated by using a quantitative structure−activity relationship (QSAR) analysis based on a linear expression by representative energy terms (LERE). The LERE-QSAR analysis quantitatively reveals that the variation in the observed (experimental) inhibitory potency among the arylsulfone analogs is decisively governed by those in the intrinsic binding and dispersion interaction energies. The results show that the LERE-QSAR analysis not only can excellently reproduce the observed overall free-energy change but also can determine the contributions of representative free-energy changes. An inter-fragment interaction energy difference (IFIED) analysis based on the fragment molecular orbital (FMO) method (FMO-IFIED) leads to the identification of key residues governing the variation in the inhibitory potency as well as to the understanding of the difference between the interactions of the carboxylic and hydroxamic acid zinc binding groups. The current results that lead to the optimization of the inhibitory potency of arylsulfone analogs toward MMP-12 to be used in the treatment of chronic obstructive pulmonary disease may be useful for the development of a new potent MMP-12 inhibitor.

1. Introduction

Human matrix metalloproteinases (MMPs), collectively called matrixins, are calcium-dependent and zinc-containing endopeptidases that are involved in the degradation and remodeling of various structural components of an extracellular matrix containing glycoproteins such as collagen, proteoglycans, and fibronectins.[1] MMPs play pivotal roles in connective tissue remodeling through the extracellular matrix regulation that occurs in a great variety of physiological processes like embryonic development, growth, and wound healing as well as pathological processes including inflammatory, vascular lesions, and carcinogenesis.[1–4] Under physiological conditions, in addition to regulation by activation process and gene expression, the activities of MMPs are also intrinsically regulated by four types of endogenous inhibitors called tissue inhibitors of metalloproteinases.[5,6] Pathologies such as rheumatoid arthritis, arteriosclerosis, and cancer, occur as a result of an imbalance between MMPs and tissue inhibitors of metalloproteinases.[7,8] Although tissue inhibitors of metalloproteinases were considered as potential inhibitors for the diseases mentioned above, they were rapidly surpassed by small molecule inhibitors due to the lack of selectivity and possessing its own biological functions.

MMPs have therefore been an attractive pharmaceutical target for over two decades.[9–13] Many inhibitors have been discovered in considerable research efforts and some of these have been evaluated in advanced clinical trials. However, almost all except for doxycycline hyclate (Periostat), which has been approved by the U.S. Food and Drug Administration (FDA) for the treatment of periodontal disease, failed because of no significant clinical benefit and/or adverse side effects.[13] A possible main reason for the low success rate is the difficulty of giving effectiveness and selectivity to an inhibitor. In other words, a mechanism of binding interaction

between MMPs and inhibitors at the atomic and electronic levels remains unclear. This issue can be attributed to the fact that overall structural features and catalytic domains of MMPs are generally quite similar.[14–16] Currently, MMPs from a group of 23 members in human, the structures of which have been determined, take a close topology in the active sites.[17–19] The structural similarity of MMPs makes it more difficult to develop selective inhibitors.

Among MMPs, macrophage elastase (MMP-12, EC 3.4.24.65)[20,21] was originally identified as an elastolytic metalloproteinase produced by inflammatory macrophages. MMP-12 is responsible for inflammatory diseases not only through the degradation of elastin, which is a major substrate for MMP-12 and widely distributed in lung, but also through a number of extracellular matrix components. Moreover, MMP-12 is predominantly involved in acute and chronic pulmonary inflammatory diseases associated with an intense airway remodeling, particularly observed in the pathogenesis of chronic obstructive pulmonary disease (COPD).[22–24] COPD is a heterogeneous inflammatory lung disease associated with irreversible progressive airflow limitation. The primary cause of COPD is air pollutant (*e.g.*, PM 2.5) as well as tobacco smoke. The WHO predicts that COPD will become the third leading cause of death worldwide by 2030; thus, social needs for the development of a new therapeutic agent for COPD are extremely high. It should be noted that overexpression of MMP-12 in lung tissue from patients suffering from COPD was confirmed in several studies.[25] These observations suggest that MMP-12 is a key molecule in COPD and the development of potent and highly selective MMP-12 inhibitors is useful for the treatment of COPD.

Comprehensive reviews[26–28] on a classical quantitative structure−activity relationship (QSAR) study as to the inhibitory potency of a series of MMP inhibitors against various types of MMPs have been reported. In addition, a correlation analysis based on a linear expression by

representative energy terms (LERE)-QSAR approach[29] and computational ones[30–40] have also been reported. The LERE-QSAR approach successfully revealed the quantitative contribution of each representative energy term to the variation in the binding affinity among MMP-9 inhibitors. Almost all of these studies discussed the inhibition mechanism of MMP-2, MMP-3, and MMP-9, all of which are implicated in tumor invasion and metastasis in cancer, while the mechanism of MMP-12 was rarely found in the reports. This is because MMP-12 is a rare MMP that is known to be exerted anti-cancer effects.[41] However, MMP-12 is a potentially important target for COPD; therefore, it is of great importance to elucidate the binding interaction mechanism of MMP-12 with its inhibitors by means of the LERE-QSAR analysis.

In this work, we performed the LERE-QSAR analysis to examine the binding mechanism of MMP-12 inhibitors at the atomic and electronic levels. Although the development of "selective" MMPs inhibitors is a crucial task as mentioned above, this study focuses on the determination of the energetic and structural factors that contribute to "potent" MMP-12 inhibitors. For this purpose, eight arylsulfone inhibitors of MMP-12, which have two types of carboxylic and hydroxamic acids as the most representative zinc binding group,[42] were selected. The eight inhibitors with the two types of zinc binding groups from Nuti *et al.*[42] were chosen to (1) provide a reasonable dynamic range of experimental free-energy changes for the validation of the application range of the LERE-QSAR analysis, (2) clarify the difference between the inhibitory potencies (chelating properties) of the carboxylic and hydroxamic acid zinc binding groups, and (3) avoid a complicated discussion by excluding racemates from the compound set. The number of inhibitors we examined here is too small to obtain a new perspective on drug discovery; however, the understanding of the binding mechanism of these inhibitors with MMP-12 that is obtained from the LERE-QSAR analysis is considered to be a clue for drug design. Herein,

MMP-12−inhibitor complexes were constructed by docking simulations and quantum mechanics and molecular mechanics (QM/MM) calculations. Then energetic contributions that govern the variation in the inhibitory potency among the inhibitors were determined by the LERE-QSAR analysis. This strategy may be useful for the development of new drugs for COPD involving MMP-12.

2. Methods

2.1. Compound set

Table 1 lists the chemical structures of eight arylsulfone analogs examined in this study along with their inhibitory potencies against MMP-12,[42] characterized by 50% inhibitory concentration (IC_{50}) at 37 °C. The compounds are classified into two types based on their zinc binding group; type **I** (compounds **1**–**4**) have a carboxylic acid (COO^-) and type **II** (compounds **5**–**8**) have a hydroxamic acid ($CONHO^-$) as substituent R_1. The types **I** and **II** compounds possess four kinds of aryl substituents (R_2 = *p*-methoxy phenyl, *p*-methoxy diphenyl ether, diphenyl, and *p*-methoxy diphenyl). Thus, a total of eight compounds with the common skeletal structure of a benzenesulfonyl scaffold were subjected to analyses.

[Table 1]

2.2. Modeling of complex structures

Although a number of crystallographic structures of MMP-12 complexed with an inhibitor have been resolved, no complex structure of MMP-12 with the identical arylsulfone inhibitor is currently available. The crystallographic structure of the catalytic domain of MMP-

12−biphenylsulfonamide hydroxamic acid complex (PDB code: 3F17)[43] was taken as the initial geometry because it possesses the highest resolution of 1.10 Å among all the structures of MMP-12, and its inhibitor is structurally similar to the arylsulfone inhibitors. As shown in Fig. 1, MMP-12 contains a catalytic zinc ion (Zn_{cat}^{2+}) coordinated by three His residues (His218, His222, and His228), which is a target for the zinc binding group in the inhibitors. Besides Zn_{cat}^{2+}, there are a structural zinc ion (Zn_{str}^{2+}) tetrahedrally coordinated by three His and one Asp residues (His168, His183, His196, and Asp170) and three structural calcium ions (Ca_{I}^{2+}, Ca_{II}^{2+}, and Ca_{III}^{2+}), which commonly contribute to the structural stability of MMPs (see also Fig. S1 in ESI). These metal ions and most of the crystallographic water molecules were retained in the protein. In the complex of 3F17, the inhibitor and a part of crystal water molecules that prevent a conformational search of the arylsulfone inhibitors were removed for the following docking simulations. Several experimental and theoretical studies[44–46] have demonstrated that inhibitors with a hydroxamic acid zinc binding group lose their hydroxyl proton to a catalytic glutamic acid in the active site of zinc-containing enzymes upon complex formation with a catalytic zinc ion, even though target enzymes are tumor necrosis factor-α converting enzyme and MMPs other than MMP-12. Given the similarities in the active sites among these zinc-containing enzymes, it is quite probable that the proton transfer from zinc binding groups of inhibitors to the catalytic glutamic acid (corresponding to Glu219 in MMP-12) also occurs in MMP-12. According to the final step of the binding mechanism proposed by Cross *et al.*,[45] both the carboxylic and hydroxamic acid zinc binding groups were deprotonated (anionized form), and one of the carboxylate oxygens of Glu219 was protonated (neutral form). The mutated amino acid residue, Asp171, was located in the vicinity of the active site of MMP-12, the side chain of which was replaced by that of Phe171 in the wild-type MMP-12.

After the preparation of the receptor structure, docking simulations were performed by using CHARMm-based DOCKER (CDOCKER)[47] implemented in Discovery Studio 3.5 for the exploration of the binding mode of the eight compounds. The docking procedure consists of the following four steps: (i) The docking site of MMP-12 was defined by using the position of the reference inhibitor (biphenylsulfonamide hydroxamic acid) and further manually modified depending on the size of the compounds. (ii) 1000 random conformations were generated for the compounds and subjected to simulated annealing molecular dynamics in the rigid active site of MMP-12 wherein temperature and the rest of the parameters were set to the default values. (iii) A full energy minimization was used to refine the resulting poses. (iv) From the 1000 binding modes, the complex structure with the highest docking score (CDOCKER energy) was selected as the most probable complex for each compound. It should be noted that the examined compounds are used as a zinc chelating inhibitor, *i.e.*, both the carboxylic and hydroxamic acid zinc binding groups chelate Zn_{cat}^{2+} in the docking simulations. The assumption we are dealing with is based on the study of Nuti *et al.*,[42] where they clearly demonstrated that the hydroxamic acid type of compound (corresponding to compound **6**) is not a non-zinc chelating MMP inhibitor but a zinc chelating inhibitor, using the combined approach of docking and NMR studies. With regards to the carboxylic acid type of compound, it probably acts as a zinc chelating inhibitor,[48] although the corresponding NMR study was not conducted. These observations and speculations are also confirmed in the available experimental structures of MMP-12 complexed with ligands bearing the carboxylic acid[49,50] as well as the hydroxamic acid.[51–53] The superimposition of complex structures of MMP-12 suggests that the carboxylic and hydroxamic acid groups chelate Zn_{cat}^{2+}. From verification of the binding modes of the two types of compounds (see Table S1 in ESI), we think that these compounds actually inhibit MMP-

12 as a zinc chelating inhibitor where the carboxylic and hydroxamic acids chelate Zn_{cat}^{2+} through different binding mechanism.

Next, the first ranked complex for each compound resulting from the docking simulations was subjected to a sophisticated minimization to consider protein flexibility. Before the energy minimization, the following preparation for the complexes was performed. There are two main approaches to model the potentials of metal ions in metalloenzymes: a bonded model and a nonbonded model. According to the work of Marcial *et al.*,[54] catalytic and structural zinc ions (Zn_{cat}^{2+} and Zn_{str}^{2+}) were used in hybrid bonded/nonbonded and bonded models, respectively. Zn_{cat}^{2+} was covalently linked to the epsilon nitrogen (Nε) atoms of His218, His222, and His228, whereas Zn_{cat}^{2+}−arylsulfone inhibitor interaction was described through the nonbonded model. On the other hand, Zn_{str}^{2+} was covalently linked to the Nε atoms of His168, His183, and His196, and the delta oxygen (Oδ) atom of Asp170. All the parameters were taken from the literature.[54] For three calcium ions (Ca_I^{2+}, Ca_{II}^{2+}, and Ca_{III}^{2+}), we used the nonbonded representation proposed by Åqvist.[55] The protonation states of His residues other than the Zn^{2+}-bonded His ones mentioned above were determined at pH 7.0 by using the PDB2PQR web server,[56] and those of Arg, Lys, Asp, and Glu residues having ionizable side chains other than Asp170 and Glu219 were treated as charged entities. The partial atomic charges in the compounds were determined according to the restrained electrostatic potential (RESP)[57] fitting procedure with the Hartree−Fock (HF)/6-31G(d) calculations (Gaussian 09 program package).[58] The resulting complex structures were solvated in a truncated octahedral box of TIP3P waters extending 12 Å from MMP-12, and seven chloride ions (Cl^-) were added for the neutralization of the systems. Four-step energy minimizations were then performed as follows: (i) the hydrogen atoms of all residues and the side chain atoms of the replaced Phe171, (ii) water molecules and ions, (iii) the

side chain atoms of all residues, and (iv) all atoms were sequentially relaxed for 2000, 5000, 5000, and 5000 steps, respectively. During these minimizations, the distances and dihedral angles between the coordinating atoms of the zinc binding groups (R_1) and Zn_{cat}^{2+} were constrained at crystallographic average values (see Table S1), which were obtained from the several experimental structures of MMP-12 with ligands having the carboxylic and hydroxamic acid zinc binding groups. The constraint is because the predicted binding modes of the zinc binding groups were not close to the crystallographically observed ones or at least unacceptable, that is, implying difficulties to predict the accurate binding mode of the zinc binding groups to Zn_{cat}^{2+} without any constraints.[59,60] All molecular mechanics calculations were carried out by using the AMBER10 package[61] with the parameters of parm99[62] and general AMBER force field (GAFF)[63] for MMP-12 and the compounds, respectively.

A two-layer QM/MM (our own *N*-layered integrated molecular orbital and molecular mechanics: ONIOM)[64] approach with the mechanical embedding (ME) scheme was used for further structural refinement of the minimized complex structures of MMP-12 with the eight compounds. The QM region consists of Zn_{cat}^{2+}, the side chain atoms of His218, His222, His228, and Glu219, all the atoms of Leu181 and Ala182, the entire compound, and one water molecule in the active site, as illustrated in Fig. 1. A number of crystallographic complex structures of MMP-12 revealed that this bridging water molecule plays an important role in the binding interaction through the hydrogen-bonding network with Ala184, Glu219, and zinc binding groups of ligands. Hence, we constructed all the complexes by keeping the water molecule in the active site as a part of the structure of MMP-12. All other water molecules were removed in the QM/MM calculations. The QM region of the system was described at the semi-empirical method PM6,[65] followed by the HF/6-31G(d) calculation; the MM region was described by using the

parameters of parm99 and GAFF. All atoms other than those in the zinc binding groups of the compounds in the QM region and a part of atoms in the active site residues in the MM region of the complexes were allowed to move without any constraints, whereas atoms in the zinc binding groups and the others in the MM region were frozen. The constraint of the zinc binding groups was done because the fact that an even unconstrained QM/MM minimization resulted in a local geometry that was in unsatisfactory agreement with the crystallographic structure, as reported by Toba *et al.*[66] The complex structures obtained from the procedure mentioned above were used for the calculation of representative energy terms in the LERE-QSAR analysis. QM/MM geometry optimizations were performed by using the Gaussian 09 program package.[58]

[Fig. 1]

2.3. Formulation of LERE-QSAR equation

Details of the formulation of the LERE-QSAR equation and its applications can be found in a review article[67] and reports of case studies,[29,68–71] respectively. We provide a brief summary of LERE-QSAR here. The LERE-QSAR equation is formulated based on the following three assumptions: (I) additivity of free-energy changes, (II) LERE approximation, and (III) entropy−enthalpy compensation rule. The first assumption is that the free-energy terms comprising the overall free-energy changes associated with complex formation between a congeneric series of ligands and their target protein are all additive.[72,73]

$$\Delta G_{obs} = \Delta G_{bind} + \Delta G_{sol} + \Delta G_{others} \text{ (additivity assumption)} \quad \text{(I)}$$

ΔG_{obs} on the left-hand side of eq I is the observed overall free-energy change obtained from the experimental inhibitory potency C ($\Delta G_{obs} = RT \ln C$, where C is the IC_{50} in this study). ΔG_{bind} and ΔG_{sol} are the binding free-energy of a ligand with a protein and the solvation free-energy change associated with complex formation, respectively. ΔG_{others}, the sum of free-energy terms other than ΔG_{bind} and ΔG_{sol}, is assumed to be linear with that of representative free-energy terms.

$$\Delta G_{others} = \beta (\Delta G_{bind} + \Delta G_{sol}) + const \text{ (LERE approximation)} \quad \text{(II)}$$

where ΔG_{others} is expected to work as a penalty term ($\beta < 0$ and/or $const > 0$),[74–76] as demonstrated in the previous works.[67,69] The third assumption is the entropy−enthalpy compensation rule,[77–81] which is expected to effectively hold for the binding of a series of ligands with a protein.

$$T\Delta S_{obs} = \alpha \Delta H_{obs} + const \text{ (entropy−enthalpy compensation rule)} \quad \text{(III)}$$

where $\alpha > 0$. From this rule, ΔG_{bind} and ΔG_{sol} can be expressed as the effective enthalpic changes. ΔG_{bind} ($\approx \Delta E_{bind}$ in solution) consists of ΔE_{bind}^{0} and E_{disp}, which are the intrinsic binding and dispersion interaction energies, respectively. ΔG_{sol} is replaceable by its dominant polar contribution ΔG_{sol}^{polar}, which comes mostly from the enthalpic contribution.[82] The combination of the three equations (assumptions) yields the following general expression:

$$\Delta G_{obs} = \gamma (\Delta E_{bind}^{0} + E_{disp} + \Delta G_{sol}^{polar}) + const \text{ (LERE-QSAR equation)} \quad \text{(IV)}$$

The coefficient γ (= $(1 - \alpha)(1 + \beta)$) on the right-hand side of eq IV is a constant determined by α and β. LERE-QSAR should also be called "linear scaling of representative energy terms" due to the fact that ΔG_{obs} is predicted by linear scaling of the representative energy terms in a generalized form of the equation.[83,84]

2.4. Calculation of representative energy terms

The intrinsic binding energy ΔE_{bind}^{0} (= E(complex) – [E(ligand) + E(protein)]) was calculated at the ONIOM(HF/6-31G(d):Amber) level with the mechanical embedding (ME) and electronic embedding (EE) schemes, which are denoted as $\Delta E_{bind}^{ONIOM/HF/ME}$ and $\Delta E_{bind}^{ONIOM/HF/EE}$, respectively. ΔE_{bind}^{0} was also calculated by using the *ab initio* fragment molecular orbital (FMO)[85–87] calculations at the HF/6-31G(d) level ($\Delta E_{bind}^{FMO/HF}$) with the GAMESS program package.[88] A detailed description on how to treat ion blocks in the FMO calculations is shown in Fig. S1. In order to obtain the dispersion interaction energy E_{disp}, all the HF energies were corrected for dispersion forces by using the Grimme's dispersion correction scheme D3,[76,89–91] which is computationally inexpensive but can reasonably account for E_{disp}.[92,93] The polar solvation free-energy change ΔG_{sol}^{polar} was calculated with the continuum solvation model based on the generalized Born (GB) approximation.[94] In the GB calculation the interior (solute) and exterior (solvent) dielectric constants were set to 1 and 78.39, respectively.

Molecular dynamics (MD) simulations with 2 ns of a production run on the complexes of MMP-12 with compounds **2** and **6** at 310 K were performed to assess how the representative energy terms ($\Delta E_{bind}^{ONIOM/HF/ME}$, ΔG_{sol}^{polar}, and E_{disp}) are sensitive to structural changes (fluctuations). Average complex structures were constructed from snapshot structures, which were collected for the last 200, 300, and 400 ps MD trajectory at 0.1 ps intervals, and then the

average complexes were energetically minimized according to the same procedure described in Section 2.2. As shown in Table S2, although the absolute differences between the two electrostatic energy terms ($\Delta E_{bind}^{ONIOM/HF/ME}$ and ΔG_{sol}^{polar}) of single (only MM) and average (MD + MM) minimized complexes are somewhat large, the relative absolute errors of the electrostatic terms and the sum of them as well as the dispersion term (E_{disp}) are less than 3.0%. Thus, we think that the effect of structural changes on the representative energy terms is not significant and that the result of the LERE-QSAR analysis using these energy terms is substantially unaffected by structural changes. Single minimized complex structures obtained with the modeling procedure described in Section 2.2 are enough to determine energetic contributions in the LERE-QSAR analysis.

2.5. Inter-fragment interaction energy analysis

The inter-fragment interaction energy (IFIE) is one of the most advantageous outcomes directly obtained with the FMO procedure because it can represent the interaction energy between a ligand and an amino acid residue in a protein.[95,96] In the present study, however, it is impossible to directly obtain IFIE values between an arylsulfone inhibitor and residues due to the bonded treatment of the arylsulfone inhibitor−Zn_{cat}^{2+} block in the FMO calculations (Fig. S1). We therefore introduced the IFIE difference term (IFIED(i, j)), which can quantitatively estimate the interaction energy of an arylsulfone inhibitor (i-th fragment) with residues (j-th), according to the work of Yoshida *et al.*[68]

$$\mathrm{IFIED}(i,j) = \mathrm{IFIE}_{\mathrm{complex}}(k,j) - \mathrm{IFIE}_{\mathrm{protein}}(l,j) \quad \text{(V)}$$

where $IFIE_{complex}(k, j)$ and $IFIE_{protein}(l, j)$ are the IFIE values of the j-th fragment with the arylsulfone inhibitor−Zn_{cat}^{2+} (k-th) and Zn_{cat}^{2+} blocks (l-th), respectively. IFIED(i, l), which cannot be directly obtained from eq V, was estimated separately from the supermolecular calculation for an arylsulfone inhibitor−Zn_{cat}^{2+} block model extracted from the QM/MM minimized complex structure (IFIED(i, l) = E(arylsulfone inhibitor−Zn_{cat}^{2+} block) − [E(arylsulfone inhibitor) + E(Zn_{cat}^{2+} block)]). ΣIFIED(i, j) represents the sum of the IFIED(i, j) values for all the j-th fragments including IFIED(i, l) one.

3. Results and discussion

3.1. Classical QSAR and docking analyses on arylsulfone analogs

We first performed a classical QSAR analysis on the eight compounds using hydrophobicity (Clog P) and molar refractivity (MR) parameters,[97] which were demonstrated to be the most important determinants of the activities of MMPs by Verma and Hansch.[28] Because Clog P and MR parameters are almost comparable in the current case due to the high correlation with each other (r = 0.973), Fig. 2a shows a plot between ΔG_{obs} and Clog P values instead of MR. The negative slope values of the two lines in Fig. 2a indicate that the inhibitory potencies of the two types of compounds increase with an increase in their hydrophobicity. Although Clog P values of the type **I** compounds **1**–**4** (having a carboxylic acid) and the type **II** compounds **5**–**8** (having a hydroxamic acid) are linearly correlated with ΔG_{obs} (r = −0.940 and −0.733, respectively), no correlation is observed for the total eight compounds. The result of the classical QSAR analysis suggests that Clog P and MR parameters cannot give an unequivocal interpretation as to the difference between the inhibitory potencies of the two types of compounds.

Next, we performed a docking analysis using CDOCKER to predict the inhibitory potency as well as to examine the binding mode of the eight compounds. As can be seen in Fig. 2b, the docking result shows similar features to those of the classical QSAR one. The CDOCKER energies of the first ranked types **I** and **II** complexes are correlated with ΔG_{obs} (r = 0.299 and 0.921, respectively) although the correlation of the type **I** complexes is considerably poor, showing that stabilization of the binding energies increases the inhibitory potencies. The use of CDOCKER interaction energies (excluding the intra-molecular energy for ligands) instead of the CDOCKER energies significantly improved the correlation quality of the type **I** complexes from r = 0.299 to 0.894 (data not shown), but the prediction of the inhibitory potency of all the compounds still remained inaccurate. Unreliable results are attributable to inconsistency between the predicted and crystallographically observed binding modes of the zinc binding groups, as summarized in ESI, Table S1 and Fig. S2. The predicted binding modes of the zinc binding groups are quite dissimilar compared to those observed in experimental structures. Probably the reason of this error lies in potential problems associated with Zn_{cat}^{2+} as well as in the large size and in the high degree of freedom of the examined compounds. In fact, visual inspection of Fig. S2 indicates that geometrical differences in the compounds come mainly from those in the zinc binding groups. Although there are somewhat root mean square deviations between the first ranked pose (highest docking score) and the other top 10 ranked poses (see Table S3), we finally selected the first ranked pose in which the zinc binding group shows a similar geometry to that of the experimental structure. However, a slight incorrectness in docked geometries cannot give accurate binding energies, so the further QM/MM minimization that can handle the polarization effect and charge redistribution surrounding Zn_{cat}^{2+} is needed to support the reliability of the docking simulations and to give the reliable binding modes of the zinc binding groups.

The classical QSAR and docking analyses did not allow us to distinguish between the inhibitory potencies of the two types of compounds having the carboxylic and hydroxamic acid zinc binding groups.

[Figs. 2a, 2b, and 2c]

3.2. Catalytic binding mode of arylsulfone analogs to MMP-12

QM/MM geometry optimizations for the first ranked complexes resulted in the consistent complex structures of the zinc binding groups in the compounds with the catalytic zinc ion in MMP-12. The optimized structures nicely reproduced experimental geometries for the catalytic zinc ion (Zn_{cat}^{2+})/inhibitor coordination system. Table 2 lists the distances and angles around the Zn_{cat}^{2+} block for all the optimized complexes in comparison with those average values for the experimental structures of MMP-12 with ligands having the carboxylic and hydroxamic acid zinc binding groups. The calculated distances and angles are in good agreement with the experimental ones. The average distances between the two oxygen (O1 and O2) atoms of the carboxylic acid zinc binding group in the type **I** compounds and Zn_{cat}^{2+} are 2.00 and 2.68 Å, respectively, which indicates that the carboxylic acid acts as a monodentate ligand with nonequivalent O−Zn_{cat}^{2+} distances. In the type **II** compounds, on the other hand, the corresponding distances (O1−Zn_{cat}^{2+} and O2−Zn_{cat}^{2+}) are 2.11 and 2.16 Å, respectively, which indicates that the hydroxamic acid acts as a bidentate ligand with equivalent O−Zn_{cat}^{2+} distances. As well known, the carboxylic acid can take monodentate binding mode exhibiting tetrahedral (TH) coordination sphere around Zn_{cat}^{2+}, while the hydroxamic acid can take trigonal bipyramidal (TB)/square-based pyramid (SP) coordination sphere. For the type **I** compounds having the carboxylic acid, the TH coordination

sphere that is composed of only the O1 (one of the carboxylate oxygens) atom of the type **I** compounds, the Nε atoms of three His residues (His218, His222, and His228), and Zn_{cat}^{2+} is commonly found because the O2 atom is far away from Zn_{cat}^{2+}. The coordination sphere for the type **II** compounds having the hydroxamic is supposed to be TB, judging from the comparison of calculated angles with the ideal values for TB and SP (shown in Table 2). The coordination of Zn_{cat}^{2+} is supported by the interaction of the zinc binding group where oxygen atoms of both the carboxylic and hydroxamic acids commonly participate in hydrogen-bond formation with the protonated side chain of the catalytic Glu219 and the water molecule. The hydrogen atom of the NH group in the hydroxamic acid of the type **II** compounds can additionally form hydrogen-bond with the backbone oxygen atom of Ala182. With regards to the sulfonyl oxygen atom of the common benzenesulfonyl scaffold, it also forms hydrogen-bonds with the backbone NH atoms of Leu181 and Ala182, while the aryl moiety undergoes the dispersion type of interaction with a hydrophobic pocket (the details described in Section 3.4.2). Although the interactions occurring in the close vicinity of the catalytic zinc ion significantly stabilize complex formation of the arylsulfone inhibitors with MMP-12, it is unclear whether or not the stabilization essentially contributes to the variation in the inhibitory potency among the inhibitors.

[Table 2]

3.3. LERE-QSAR analysis of complex formation of MMP-12 with arylsulfone analogs

Here, let us consider the contribution of the representative energy terms to the variation in the observed overall free-energy change (ΔG_{obs}) associated with complex formation of MMP-12 with the arylsulfone inhibitors. Table 3 lists observed and calculated overall free-energy changes

along with the representative energy terms obtained from the calculation of the QM/MM optimized complex structures. The LERE-QSAR analysis using eq IV for the three intrinsic binding energy terms, $\Delta E_{\text{bind}}^{\text{ONIOM/HF/ME}}$, $\Delta E_{\text{bind}}^{\text{ONIOM/HF/EE}}$, and $\Delta E_{\text{bind}}^{\text{FMO/HF}}$, gave nice correlation eqs 1, 2, and 3, respectively.

$$\Delta G_{\text{obs}} = 0.226\ (\Delta E_{\text{bind}}^{\text{ONIOM/HF/ME}} + E_{\text{disp}} + \Delta G_{\text{sol}}^{\text{polar}}) + 16.9 \quad (1)$$

$n = 8$, $r = 0.968$, $r_{\text{cv}} = 0.937$, $s = 0.670$, $s_{\text{cv}} = 0.806$, $F = 88.5$

$$\Delta G_{\text{obs}} = 0.235\ (\Delta E_{\text{bind}}^{\text{ONIOM/HF/EE}} + E_{\text{disp}} + \Delta G_{\text{sol}}^{\text{polar}}) + 16.0 \quad (2)$$

$n = 8$, $r = 0.961$, $r_{\text{cv}} = 0.920$, $s = 0.739$, $s_{\text{cv}} = 0.900$, $F = 71.8$

$$\Delta G_{\text{obs}} = 0.187\ (\Delta E_{\text{bind}}^{\text{FMO/HF}} + E_{\text{disp}} + \Delta G_{\text{sol}}^{\text{polar}}) + 11.5 \quad (3)$$

$n = 8$, $r = 0.956$, $r_{\text{cv}} = 0.918$, $s = 0.782$, $s_{\text{cv}} = 0.915$, $F = 63.4$

As shown in Fig. 2c, the variation of ΔG_{obs} is excellently reproducible with the LERE-QSAR analysis in contrast to the classical QSAR and docking ones in Section 3.1 (shown in Fig. 2a and 2b, respectively). In addition to a regression analysis with statistical parameters (r, s, and F), the correlation equations were validated by using leave-one-out cross-validation and an external test set of compounds that were not used in the model development. The cross-validated correlation coefficients (r_{cv}) in eqs 1–3 are all more than 0.91 and the corresponding standard errors (s_{cv}) are all less than 0.92, suggesting that the equations are predictive and statistically significant. Furthermore, these equations were used to predict the test set of four compounds not involved in the regression analysis. The chemical structures, experimental values, and prediction results of

the external test set are given in Table S4 and Fig. S3. The predictive correlation coefficients for the test set in eqs 1–3 are all more than 0.86, indicating a good predictive power of the constructed models. Fig. S3 illustrates the agreement between ΔG_{obs} and ΔG_{calc} for the training (internal) and test (external) sets as well as the predictive power of eqs 1–3. The validations suggest that the LERE-QSAR models are useful and have a good internal and external predictive power. The statistical qualities of all the correlation equations are almost same. The uses of $\Delta E_{bind}^{ONIOM/HF/EE}$ and $\Delta E_{bind}^{FMO/HF}$ slightly decreased the correlation compared with that of $\Delta E_{bind}^{ONIOM/HF/ME}$ because the polarization energy (= $\Delta E_{bind}^{ONIOM/HF/EE} - \Delta E_{bind}^{ONIOM/HF/ME}$) and many-body polarization effects were not statistically significant in the current case. Fig. 3 shows the variations in the representative energy terms used in eq 1. The variances (**I** + **II**) of $\Delta E_{bind}^{ONIOM/HF/ME}$ and ΔG_{sol}^{polar} are considerably large (417 and 152 kcal^2/mol^2, respectively, shown in Table 3). However, it should be noted that the large values are due to differences between the interactions of the types **I** and **II** compounds but not from those within each type of compound. Actually, both the variances (**I**) and (**II**) of the two electrostatic energy terms are considerably small ($\Delta E_{bind}^{ONIOM/HF/ME}$: 6.12 (**I**) and 2.70 (**II**); ΔG_{sol}^{polar}: 6.44 (**I**) and 3.65 (**II**) kcal^2/mol^2). The situation can be clearly seen in Fig. 3, where the two electrostatic energy terms discriminate the interaction energies between the types **I** and **II** compounds, and moreover compensate each other (r = −0.971). The anti-correlation means that stabilization by $\Delta E_{bind}^{ONIOM/HF/ME}$ counteracts destabilization by ΔG_{sol}^{polar} nonlinearly and the stabilization contribution overwhelms the destabilization one. On the other hand, the variances (**I**) and (**II**) of E_{disp} (76.8 and 69.6 kcal^2/mol^2, respectively) are considerably larger than those of the two electrostatic energy terms. E_{disp} of the types **I** and **II** compounds shows a nice correlation with ΔG_{obs} (r = 0.954 and 0.946, respectively), but the correlation for the total eight compounds is

poor (r = 0.572). This result indicates that the variation of E_{disp} governing ΔG_{obs} does not come from the dispersion interaction energies of the zinc binding group (R_1) and the benzenesulfonyl scaffold (common skeletal structure), but rather from that of the aryl substituent (R_2) because each type of compound is different only in R_2. Consequently, the variations of $\Delta E_{bind}^{ONIOM/HF/ME}$ and E_{disp} are predominant contributors to that of ΔG_{obs}. In fact, the sum of $\Delta E_{bind}^{ONIOM/HF/ME}$ and E_{disp} (ΔE_{bind}, total binding energy) is nicely correlated with ΔG_{obs} among the total eight compounds (r = 0.945, n = 8) as well as among each type of compound (r = 0.961 for type **I** and 0.917 for type **II**). The results mentioned above clearly suggest that the intrinsic binding energy is most crucial for distinguishing the difference in the observed overall free-energy change between the two types of zinc binding groups and that the dispersion interaction energy is for the variation among the four kinds of aryl substituents.

In summary, the binding interaction energy of the arylsulfone inhibitor with MMP-12 decisively governs the variation in the inhibitory potency.

[Table 3]

[Fig. 3]

3.4. Contributions of individual interaction energies of arylsulfone analogs with amino acid residues to total binding energy

To further understand the detailed interaction mechanism of the MMP-12−arylsulfone inhibitor complex and to identify the key residues governing the variation in the inhibitory potency, we applied the FMO-IFIED analysis to decompose the total binding energy ΔE_{bind} (= $\Delta E_{bind}^{FMO/HF} + E_{disp}$), which is the most dominant energetic term, into the interaction energies of

the arylsulfone inhibitor with amino acid residues in MMP-12 (the binding water molecule is taken as a residue of MMP-12). As expected,[68,70,95] there is an almost complete linearity between ΔE_{bind} and ΣIFIED (ΔE_{bind} = 0.929 ΣIFIED − 19.8, n = 8, r = 1.000), suggesting that the FMO-IFIED analysis allows us to clarify the quantitative contribution of each amino acid residue to ΔE_{bind}. Fig. 4a shows the IFIED values of amino acid residues with compounds **2** and **6**, which have the same aryl substituent (*p*-methoxy diphenyl ether) and exhibit the high activity toward MMP-12 within each type of compound. Large absolute IFIED values come from the strong electrostatic interactions of the compounds with charged amino acid residues. The IFIED (arylsulfone inhibitor, Zn_{cat}^{2+} block) values are the largest among them, and the contributions reach more than 60% of ΣIFIED (see Table S5). Fig. 4b shows the variances of the IFIED values among the total eight compounds as well as among each type of compound. The profiles of the variances reflect the presence of the two types of interaction modes arising from the difference between the two types of zinc binding groups (R_1) and variation among the four kinds of aryl substituents (R_2). The difference between the two types of zinc binding groups is represented by some large peaks of only the variance (**I** + **II**), while variation among the four kinds of aryl substituents is represented by those of both the variances (**I**) and (**II**). These peaks with the variance larger than 1.4 $kcal^2/mol^2$ are the following residues (fragments): Ala182, the water molecule, one calcium (Ca_{III}^{2+}), and two zinc ion (Zn_{str}^{2+} and Zn_{cat}^{2+}) blocks for the difference between the two types of zinc binding groups; Leu214, Thr215, Val235, Met236, Tyr240, and Lys241 for variation among the four kinds of aryl substituents. The larger values of the variance are supposed to govern the variation in the total binding energy.

[Figs. 4a and 4b]

3.4.1. Contributions that determine difference between carboxylic and hydroxamic acid zinc binding groups

In this section, let us look at the contribution of the two types of zinc binding groups. Among Ala182, the water molecule, Ca_{III}^{2+}, Zn_{str}^{2+}, and Zn_{cat}^{2+} blocks, the Zn_{cat}^{2+} block exhibits the largest variance (317 $kcal^2/mol^2$), revealing that the variance of ΔE_{bind} comes mostly from the difference between the interaction energies of the types **I** and **II** compounds with the Zn_{cat}^{2+} block. The decisive contributions attributable to the difference of the carboxylic and hydroxamic acid zinc binding groups are clearly observed as significant differences in the IFIED values shown in Fig. 5a. An average value of IFIED (type **II** compounds, Zn_{cat}^{2+} block) is 35 kcal/mol more stable than that of IFIED (type **I** compounds, Zn_{cat}^{2+} block) (−272 ± 2.47 and −237 ± 1.05 kcal/mol, respectively). This result indicates that the hydroxamic acid is more favorable for binding to Zn_{cat}^{2+} through the bidentate mode with the two oxygens, which differs from the monodentate mode with the one oxygen atom of the carboxylic acid, as shown in Fig. 5b. Although there are contributions from Ala182, the water molecule, Ca_{III}^{2+}, and Zn_{str}^{2+} blocks, the differences between average IFIED values of the types **I** and **II** compounds with these residues (3.37, −6.19, −0.921, and −7.35 kcal/mol, respectively) are not great compared with the Zn_{cat}^{2+} block. Among them, the water molecule and Ala182 undergo direct interactions with the arylsulfone inhibitor where the zinc binding group and the benzenesulfonyl scaffold in the compounds form hydrogen-bond with the water molecule and the main chain of Ala182, respectively. These energetic findings can be confirmed in Fig. 5a. Interestingly, although the catalytic Glu219 also undergoes the hydrogen-bonding interactions with the zinc binding groups, the contribution to the variance of ΔE_{bind} is not significant. As shown in Fig. 4a, there are other

charged residues associated with electrostatic attractive/repulsive interactions with the negatively charged zinc binding groups in the arylsulfone inhibitors. These stabilization/destabilization energies are somewhat large but they do not make a significant difference in the interaction energy between the two types of complexes (see also Fig. 4b), suggesting that the long distance natures of electrostatic interactions of the carboxylic and hydroxamic acids with charged residues are almost same.

In any event, in total, ΔE_{bind} of the type **II** compounds is about 40 kcal/mol more stable than that of the type **I** compounds as a result of differences in the interaction energies. This is mainly due to the significant difference between the electrostatic interaction energies of the carboxylic and hydroxamic acid zinc binding groups with the catalytic zinc ion, and the difference decisively distinguishes that in the observed overall free-energy change between the two types of zinc binding groups.

[Figs. 5a and 5b]

3.4.2. Contributions that govern variation among aryl substituents

Let us next look at the contribution of the four kinds of aryl substituents. Fig. 6a shows the IFIED values of the compounds with Leu214, Thr215, Val235, Met236, Tyr240, and Lys241. The overall variations of the IFIED values come from those among the four kinds of aryl substituents but do not from the difference between the two types of zinc binding groups observed in the previous section. Because amino acid residues that govern the variance among the four kinds of aryl substituents are in close contact with the aryl substituents in the compounds, the contribution of the IFIED values to the variance of ΔE_{bind} is mostly due to the

dispersion interaction energies of these residues with the aryl substituents. In fact, the variance profile of the dispersion interaction energy (Fig. S4) is in good accordance with that of the total interaction energy (Fig. 4b). As shown in Fig. 6b, these residues are responsible for the formation of the hydrophobic pocket for the accommodating aryl substituents in the compounds. Val235 and Lys241 exhibit the largest comparable variances (9.94 and 10.2 $kcal^2/mol^2$, respectively) and the similar interaction profiles. IFIED (compound **2**, Val235 and Lys241) and IFIED (compound **6**, Val235 and Lys241) exhibit the largest stabilization value within the types **I** and **II** compounds, respectively. The main contribution to the stabilization comes from the effective dispersion interactions of the *p*-methoxy diphenyl ether group in compounds **2** and **6** with the side chains of Val235 and Lys241. The equivalent stabilization of IFIED (type **II** compounds, Tyr240) that is commonly found in compounds **5**–**8** is more stable than that of IFIED (type **I** compounds, Tyr240). The result suggests that the attachment of the hydroxamic acid zinc binding group to the type **II** compounds makes the sulfonyl moiety and the aryl substituent can take advantage positions for the dispersion interactions with Tyr240. Although the magnitudes of the interaction energies of the types **I** and **II** compounds with Leu214 and Thr215 are much weaker than those with the residues mentioned above, the contributions exhibit the distinct IFIED profiles depending on the aryl substituents. At any rate, the introduction of relatively large aryl substituents allows for effective dispersion interaction with the residues. On the other hand, the large destabilization commonly occurs at Met236 in the complexes probably because the larger substituents other than the *p*-methoxy phenyl group could be particularly involved in repulsive interaction with Met236 through steric effect. However, the presence of the *p*-methoxy phenyl group, as in compounds **1** and **5**, caused a significant reduction in the

inhibitory potency (see Table 1), probably due to the weakness of dispersion interaction with the key residues.

These results quantitatively reveal that the variation in the dispersion interaction energies of the aryl substituents in the compounds with its surrounding residues, especially Val235 and Lys241, mostly governs the variation in the observed overall free-energy change among the four kinds of aryl substituents and suggest that the size and position of the aryl substituents are crucial for the effective dispersion interaction with the residues.

[Figs. 6a and 6b]

4. Conclusions

In this article, we performed a LERE-QSAR analysis to examine the binding mechanism between MMP-12 and eight arylsulfone analogs having two types of carboxylic and hydroxamic acids as the most representative zinc binding group. Prior to the LERE-QSAR analysis, classical QSAR and docking analyses were applied for the prediction of the inhibitory potencies. These approaches could not give an unequivocal interpretation as to the difference between the inhibitory potencies of the two types of zinc binding groups because the approaches do not provide direct and detailed information on the atomic and electronic interactions responsible for the variation in the inhibitory potency. The LERE-QSAR analysis could excellently reproduce the variation in the observed overall free-energy change through the determination of the contributions of representative free-energy changes associated with complex formation of MMP-12 and the arylsulfone inhibitors. The stabilization of the intrinsic binding energy overwhelms the destabilization of the solvation free-energy change as a result of the counteraction of the two

electrostatic terms. This result is consistent with the previous one[29] as to the analysis for the inhibition mechanism of MMP-9 with biphenylsulfonamide inhibitors. In contrast to the previous results, the contribution of the dispersion interaction energy in addition to the intrinsic binding energy is also important. The intrinsic binding energy is most crucial for distinguishing the difference in the observed overall free-energy change between the two types of zinc binding groups, while the dispersion interaction energy is for the variation among the four kinds of aryl substituents. A FMO-IFIED analysis quantitatively revealed that the significant difference between the electrostatic interaction energies of the carboxylic and hydroxamic acids with the catalytic zinc ion decisively distinguishes the difference in the observed overall free-energy change between the two types of zinc binding groups. Also, the variation in the dispersion interaction energies of the aryl substituents in the compounds with its surrounding residues mostly governs the variation in the observed overall free-energy change among the four kinds of aryl substituents. The present results that determine the structural factors of effective inhibitor of MMP-12 may be useful for the development of new drugs for COPD involving MMP-12. We hope that the continuous work for inhibitors of other types of MMPs provides valuable information at the atomic and electronic levels to be helpful in the rational design of selective inhibitors toward individual MMP.

Acknowledgements

We thank Grants-in-Aid for Scientific Research (Nos. 22245028 and 24109014) from the Japan Society for the Promotion of Science (JSPS) and the Ministry of Education, Culture, Sports, Science and Technology of Japan (MEXT) and the MEXT Projects of “Integrated

Research on Chemical Synthesis" and "Elements Strategy Initiative to Form Core Research Center", and CREST of the Japan Science and Technology Cooperation.

Electronic supplementary information (ESI) available: Additional tables and figures for computational results in this work presented in tables S1–S5 and figures S1–S4. See DOI:

References

1 D. Sbardella, G. F. Fasciglione, M. Gioia, C. Ciaccio, G. R. Tundo, S. Marini and M. Coletta, *Mol. Aspects Med.*, 2012, **33**, 119–208.

2 C. E. Brinckerhoff and L. M. Matrisian, *Nat. Rev. Mol. Cell Biol.*, 2002, **3**, 207–214.

3 M. Egeblad and Z. Werb, *Nat. Rev. Cancer*, 2002, **2**, 161–174.

4 A. Page-McCaw, A. J. Ewald and Z. Werb, *Nat. Rev. Mol. Cell Biol.*, 2007, **8**, 221–233.

5 D. Bourboulia and W. G. Stetler-Stevenson, *Semin. Cancer Biol.*, 2010, **20**, 161–168.

6 K. Brew and H. Nagase, *Biochim. Biophys. Acta, Mol. Cell Res.*, 2010, **1803**, 55–71.

7 L. A. Liotta, P. S. Steeg and W. G. Stetler-Stevenson, *Cell*, 1991, **64**, 327–336.

8 Y. Yoshihara, H. Nakamura, K. Obata, H. Yamada, T. Hayakawa, K. Fujikawa and Y. Okada, *Ann. Rheum. Dis.*, 2000, **59**, 455–461.

9 M. Whittaker, C. D. Floyd, P. Brown and A. J. H. Gearing, *Chem. Rev.*, 1999, **99**, 2735–2776.

10 L. M. Coussens, B. Fingleton and L. M. Matrisian, *Science*, 2002, **295**, 2387–2392.

11 J. T. Peterson, *Cardiovasc. Res.*, 2006, **69**, 677–687.

12 J. Hu, P. E. Van den Steen, Q.-X. Sang and G. Opdenakker, *Nat. Rev. Drug Discovery*, 2007, **6**, 480–498.

13 B. Pirard, *Drug Discovery Today*, 2007, **12**, 640–646.

14 H. Nagase and G. B. Fields, *Biopolymers*, 1996, **40**, 399–416.

15 I. Massova, L. P. Kotra, R. Fridman and S. Mobashery, *FASEB J.*, 1998, **12**, 1075–1095.

16 V. Lukacova, Y. Zhang, M. Mackov, P. Baricic, S. Raha, J. A. Calvo and S. Balaz, *J. Biol. Chem.*, 2004, **279**, 14194–14200.

17 H. Nagase and J. F. Woessner, Jr., *J. Biol. Chem.*, 1999, **274**, 21491–21494.

18 R. Visse and H. Nagase, *Circ. Res.*, 2003, **92**, 827–839.

19 H. Nagase, R. Visse and G. Murphy, *Cardiovasc. Res.*, 2006, **69**, 562–573.

20 S. D. Shapiro, G. L. Griffin, D. J. Gilbert, N. A. Jenkins, N. G. Copeland, H. G. Welgus, R. M. Senior and T. J. Ley, *J. Biol. Chem.*, 1992, **267**, 4664–4671.

21 S. D. Shapiro, D. K. Kobayashi and T. J. Ley, *J. Biol. Chem.*, 1993, **268**, 23824–23829.

22 R. D. Hautamaki, D. K. Kobayashi, R. M. Senior and S. D. Shapiro, *Science*, 1997, **277**, 2002–2004.

23 G. M. Hunninghake, M. H. Cho, Y. Tesfaigzi, M. E. Soto-Quiros, L. Avila, J. Lasky-Su, C. Stidley, E. Melén, C. Söderhäll, J. Hallberg, I. Kull, J. Kere, M. Svartengren, G. Pershagen, M. Wickman, C. Lange, D. L. Demeo, C. P. Hersh, B. J. Klanderman, B. A. Raby, D. Sparrow, S. D. Shapiro, E. K. Silverman, A. A. Litonjua, S. T. Weiss and J. C. Celedón, *N. Engl. J. Med.*, 2009, **361**, 2599–2608.

24 R. Chaudhuri, C. McSharry, J. Brady, I. Donnelly, C. Grierson, S. McGuinness, L. Jolly, C. J. Weir, C. M. Messow, M. Spears, G. Miele, K. Nocka, D. Crowther, J. Thompson, M. Brannigan, J. Lafferty, M. Sproule, W. MacNee, M. Connell, J. T. Murchison, M. C.

Shepherd, G. Feuerstein, D. K. Miller and N. C. Thomson, *J. Allergy Clin. Immunol.*, 2012, **129**, 655–663.

25 S. Molet, C. Belleguic, H. Lena, N. Germain, C. P. Bertrand, S. D. Shapiro, J.-M. Planquois, P. Delaval and V. Lagente, *Inflammation Res.*, 2005, **54**, 31–36.

26 C. A. Kontogiorgis, P. Papaioannou and D. J. Hadjipavlou-Litina, *Curr. Med. Chem.*, 2005, **12**, 339–355.

27 S. P. Gupta, *Chem. Rev.*, 2007, **107**, 3042–3087.

28 R. P. Verma and C. Hansch, *Bioorg. Med. Chem.*, 2007, **15**, 2223–2268.

29 T. Yoshida, S. Hitaoka, A. Mashima, T. Sugimoto, H. Matoba and H. Chuman, *J. Phys. Chem. B*, 2012, **116**, 10283–10289.

30 S. Ha, R. Andreani, A. Robbins and I. Muegge, *J. Comput.-Aided Mol. Des.*, 2000, **14**, 435–448.

31 O. A. T. Donini and P. A. Kollman, *J. Med. Chem.*, 2000, **43**, 4180–4188.

32 T. J. Hou, W. Zhang and X. J. Xu, *J. Phys. Chem. B*, 2001, **105**, 5304–5315.

33 T. Hou, S. Guo and X. Xu, *J. Phys. Chem. B*, 2002, **106**, 5527–5535.

34 T. Hou, W. Zhang and X. Xu, *J. Comput.-Aided Mol. Des.*, 2002, **16**, 27–41.

35 R. C. Rizzo, S. Toba and I. D. Kuntz, *J. Med. Chem.*, 2004, **47**, 3065–3074.

36 A. Khandelwal, V. Lukacova, D. M. Kroll, D. Çömez, S. Raha and S. Balaz, *QSAR Comb. Sci.*, 2004, **23**, 754–766.

37 A. Khandelwal, V. Lukacova, D. M. Kroll, S. Raha, D. Comez and S. Balaz, *J. Phys. Chem. A*, 2005, **109**, 6387–6391.

38 A. Khandelwal, V. Lukacova, D. Comez, D. M. Kroll, S. Raha and S. Balaz, *J. Med. Chem.*, 2005, **48**, 5437–5447.

39 A. Khandelwal and S. Balaz, *J. Comput.-Aided Mol. Des.*, 2007, **21**, 131–137.

40 A. Khandelwal and S. Balaz, *Proteins: Struct., Funct., Bioinf.*, 2007, **69**, 326–339.

41 P. A. Konstantinopoulos, M. V. Karamouzis, A. G. Papatsoris and A. G. Papavassiliou, *Int. J. Biochem. Cell Biol.*, 2008, **40**, 1156–1168.

42 E. Nuti, L. Panelli, F. Casalini, S. I. Avramova, E. Orlandini, S. Santamaria, S. Nencetti, T. Tuccinardi, A. Martinelli, G. Cercignani, N. D'Amelio, A. Maiocchi, F. Uggeri and A. Rossello, *J. Med. Chem.*, 2009, **52**, 6347–6361.

43 I. Bertini, V. Calderone, M. Fragai, A. Giachetti, M. Loconte, C. Luchinat, M. Maletta, C. Nativi and K. J. Yeo, *J. Am. Chem. Soc.*, 2007, **129**, 2466–2475.

44 M. A. Holmes and B. W. Matthews, *Biochemistry*, 1981, **20**, 6912–6920.

45 J. B. Cross, J. S. Duca, J. J. Kaminski and V. S. Madison, *J. Am. Chem. Soc.*, 2002, **124**, 11004–11007.

46 L. Ducháčková and J. Roithová, *Chem. - Eur. J.*, 2009, **15**, 13399–13405.

47 G. Wu, D. H. Robertson, C. L. Brooks, III and M. Vieth, *J. Comput. Chem.*, 2003, **24**, 1549–1562.

48 T. Tuccinardi, E. Nuti, G. Ortore, A. Rossello, S. I. Avramova and A. Martinelli, *Bioorg. Med. Chem.*, 2008, **16**, 7749–7758.

49 M. A. Markus, B. Dwyer, S. Wolfrom, J. Li, W. Li, K. Malakian, J. Wilhelm and D. H. H. Tsao, *J. Biomol. NMR*, 2008, **41**, 55–60.

50 C. Antoni, L. Vera, L. Devel, M. P. Catalani, B. Czarny, E. Cassar-Lajeunesse, E. Nuti, A. Rossello, V. Dive and E. A. Stura, *J. Struct. Biol.*, 2013, **182**, 246–254.

51 H. Nar, K. Werle, M. M. T. Bauer, H. Dollinger and B. Jung, *J. Mol. Biol.*, 2001, **312**, 743–751.

52 I. Bertini, V. Calderone, M. Fragai, A. Giachetti, M. Loconte, C. Luchinat, M. Maletta, C. Nativi and K. J. Yeo, *J. Am. Chem. Soc.*, 2007, **129**, 2466–2475.

53 E. Attolino, V. Calderone, E. Dragoni, M. Fragai, B. Richichi, C. Luchinat and C. Nativi, *Eur. J. Med. Chem.*, 2010, **45**, 5919–5925.

54 B. L. Marcial, S. F. Sousa, I. L. Barbosa, H. F. Dos Santos and M. J. Ramos, *J. Phys. Chem. B*, 2012, **116**, 13644–13654.

55 J. Åqvist, *J. Phys. Chem.*, 1990, **94**, 8021–8024.

56 T. D. Dolinsky, J. E. Nielsen, J. A. McCammon and N. A. Baker, *Nucleic Acids Res.*, 2004, **32**, W665–W667.

57 C. I. Bayly, P. Cieplak, W. D. Cornell and P. A. Kollman, *J. Phys. Chem.*, 1993, **97**, 10269–10280.

58 M. J. Frisch, G. W. Trucks, H. B. Schlegel, G. E. Scuseria, M. A. Robb, J. R. Cheeseman, G. Scalmani, V. Barone, B. Mennucci, G. A. Petersson, H. Nakatsuji, M. Caricato, X. Li, H. P. Hratchian, A. F. Izmaylov, J. Bloino, G. Zheng, J. L. Sonnenberg, M. Hada, M. Ehara, K. Toyota, R. Fukuda, J. Hasegawa, M. Ishida, T. Nakajima, Y. Honda, O. Kitao, H. Nakai, T. Vreven, J. A. Montgomery, Jr., J. E. Peralta, F. Ogliaro, M. Bearpark, J. J. Heyd, E. Brothers, K. N. Kudin, V. N. Staroverov, R. Kobayashi, J. Normand, K. Raghavachari, A. Rendell, J. C. Burant, S. S. Iyengar, J. Tomasi, M. Cossi, N. Rega, J. M. Millam, M. Klene, J. E. Knox, J. B. Cross, V. Bakken, C. Adamo, J. Jaramillo, R. Gomperts, R. E. Stratmann, O. Yazyev, A. J. Austin, R. Cammi, C. Pomelli, J. W. Ochterski, R. L. Martin, K. Morokuma, V. G. Zakrzewski, G. A. Voth, P. Salvador, J. J. Dannenberg, S. Dapprich, A. D. Daniels, Ö. Farkas, J. B. Foresman, J. V. Ortiz, J. Cioslowski and D. J. Fox, *Gaussian 09 (Revision C.01)* Gaussian, Inc., Wallingford, CT, 2009.

59 X. Hu and W. H. Shelver, *J. Mol. Graphics Modell.*, 2003, **22**, 115–126.

60 X. Hu, S. Balaz and W. H. Shelver, *J. Mol. Graphics Modell.*, 2004, **22**, 293–307.

61 D. A. Case, T. E. Cheatham, III, T. Darden, H. Gohlke, R. Luo, K. M. Merz, Jr., A. Onufriev, C. Simmerling, B. Wang and R. J. Woods, *J. Comput. Chem.*, 2005, **26**, 1668–1688.

62 J. Wang, P. Cieplak and P. A. Kollman, *J. Comput. Chem.*, 2000, **21**, 1049–1074.

63 J. Wang, R. M. Wolf, J. W. Caldwell, P. A. Kollman and D. A. Case, *J. Comput. Chem.*, 2004, **25**, 1157–1174.

64 M. Svensson, S. Humbel, R. D. J. Froese, T. Matsubara, S. Sieber and K. Morokuma, *J. Phys. Chem.*, 1996, **100**, 19357–19363.

65 J. J. Stewart, *J. Mol. Model.*, 2007, **13**, 1173–1213.

66 S. Toba, K. V. Damodaran and K. M. Merz, Jr., *J. Med. Chem.*, 1999, **42**, 1225–1234.

67 S. Hitaoka and H. Chuman, *J. Pestic. Sci. (Tokyo, Jpn.)*, 2013, **38**, 60–67.

68 T. Yoshida, Y. Munei, S. Hitaoka and H. Chuman, *J. Chem. Inf. Model.*, 2010, **50**, 850–860.

69 Y. Munei, K. Shimamoto, M. Harada, T. Yoshida and H. Chuman, *Bioorg. Med. Chem. Lett.*, 2011, **21**, 141–144.

70 S. Hitaoka, H. Matoba, M. Harada, T. Yoshida, D. Tsuji, T. Hirokawa, K. Itoh and H. Chuman, *J. Chem. Inf. Model.*, 2011, **51**, 2706–2716.

71 S. Hitaoka, Y. Shibata, H. Matoba, A. Kawano, M. Harada, M. Rahman, D. Tsuji, T. Hirokawa, K. Itoh, T. Yoshida and H. Chuman, *Chem-Bio Informatics Journal*, 2013, **13**, 30–44.

72 U. Bren, V. Martínek and J. Florián, *J. Phys. Chem. B*, 2006, **110**, 12782–12788.

73 M. Bren, J. Florián, J. Mavri and U. Bren, *Theor. Chem. Acc.*, 2007, **117**, 535–540.

74 J. C. Faver, Z. Zheng and K. M. Merz, Jr., *J. Chem. Phys.*, 2011, **135**, 144110.

75 J. C. Faver, Z. Zheng and K. M. Merz, Jr., *Phys. Chem. Chem. Phys.*, 2012, **14**, 7795–7799.

76 H. Kruse and S. Grimme, *J. Chem. Phys.*, 2012, **136**, 154101.

77 J. D. Dunitz, *Chem. Biol. (Oxford, U. K.)*, 1995, **2**, 709–712.

78 M. S. Searle, M. S. Westwell and D. H. Williams, *J. Chem. Soc., Perkin Trans. 2*, 1995, 141–151.

79 K. N. Houk, A. G. Leach, S. P. Kim and X. Zhang, *Angew. Chem., Int. Ed.*, 2003, **42**, 4872–4897.

80 D. H. Williams, E. Stephens, D. P. O'Brien and M. Zhou, *Angew. Chem., Int. Ed.*, 2004, **43**, 6596–6616.

81 E. Freire, *Chem. Biol. Drug Des.*, 2009, **74**, 468–472.

82 R. M. Noyes, *J. Am. Chem. Soc.*, 1962, **84**, 513–522.

83 J. Åqvist, C. Medina and J. E. Samuelsson, *Protein Eng.*, 1994, **7**, 385–391.

84 J. Florián, J. Šponer and A. Warshel, *J. Phys. Chem. B*, 1999, **103**, 884–892.

85 K. Kitaura, E. Ikeo, T. Asada, T. Nakano and M. Uebayasi, *Chem. Phys. Lett.*, 1999, **313**, 701–706.

86 D. G. Fedorov, T. Nagata and K. Kitaura, *Phys. Chem. Chem. Phys.*, 2012, **14**, 7562–7577.

87 M. S. Gordon, D. G. Fedorov, S. R. Pruitt and L. V. Slipchenko, *Chem. Rev.*, 2012, **112**, 632–672.

88 M. W. Schmidt, K. K. Baldridge, J. A. Boatz, S. T. Elbert, M. S. Gordon, J. H. Jensen, S. Koseki, N. Matsunaga, K. A. Nguyen, S. Su, T. L. Windus, M. Dupuis and J. A. Montgomery, Jr., *J. Comput. Chem.*, 1993, **14**, 1347–1363.

89 S. Grimme, J. Antony, S. Ehrlich and H. Krieg, *J. Chem. Phys.*, 2010, **132**, 154104.

90 S. Grimme, S. Ehrlich and L. Goerigk, *J. Comput. Chem.*, 2011, **32**, 1456–1465.

91 T. Yoshida, A. Mashima, K. Sasahara and H. Chuman, *Bioorg. Med. Chem. Lett.*, 2014, **24**, 1037–1042.

92 U. R. Fogueri, S. Kozuch, A. Karton and J. M. L. Martin, *J. Phys. Chem. A*, 2013, **117**, 2269–2277.

93 S. R. Pruitt, S. S. Leang, P. Xu, D. G. Fedorov and M. S. Gordon, *Comput. Theor. Chem.*, 2013, **1021**, 70–83.

94 P. A. Kollman, I. Massova, C. Reyes, B. Kuhn, S. Huo, L. Chong, M. Lee, T. Lee, Y. Duan, W. Wang, O. Donini, P. Cieplak, J. Srinivasan, D. A. Case and T. E. Cheatham, III, *Acc. Chem. Res.*, 2000, **33**, 889–897.

95 S. Hitaoka, M. Harada, T. Yoshida and H. Chuman, *J. Chem. Inf. Model.*, 2010, **50**, 1796–1805.

96 C. Watanabe, K. Fukuzawa, Y. Okiyama, T. Tsukamoto, A. Kato, S. Tanaka, Y. Mochizuki and T. Nakano, *J. Mol. Graphics Modell.*, 2013, **41**, 31–42.

97 ClogP for windows ver. 4.0, BioByte Corp., 201 W. Fourth St., Suite 204, Claremot, CA 91711 USA.

Tables

Table 1 Chemical structure and inhibitory potency of arylsulfone analogs toward MMP-12

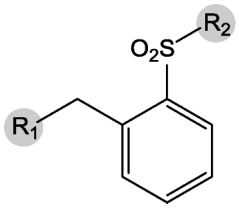

compound				MMP-12
no.	type	R_1	R_2	IC_{50}[a]
1	**I**	carboxylic acid[b]	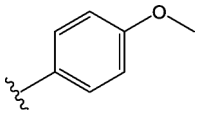	89000
2	**I**	carboxylic acid[b]	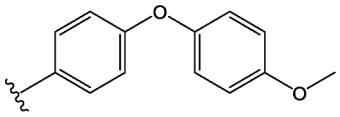	380
3	**I**	carboxylic acid[b]	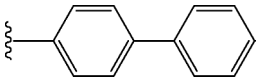	1500
4	**I**	carboxylic acid[b]	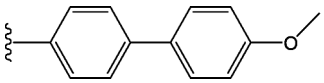	140
5	**II**	hydroxamic acid[c]	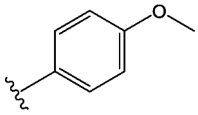	32
6	**II**	hydroxamic acid[c]	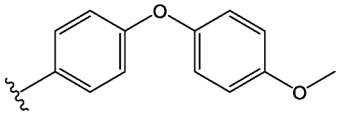	0.2
7	**II**	hydroxamic acid[c]	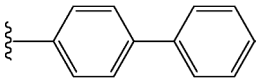	6
8	**II**	hydroxamic acid[c]	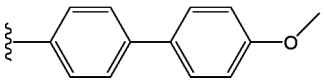	4.8

[a] Taken from ref 42 (In nM).

[b] COO^-.

[c] $CONHO^-$.

Table 2 Structural data for calculated and experimental geometries around the catalytic zinc ion block

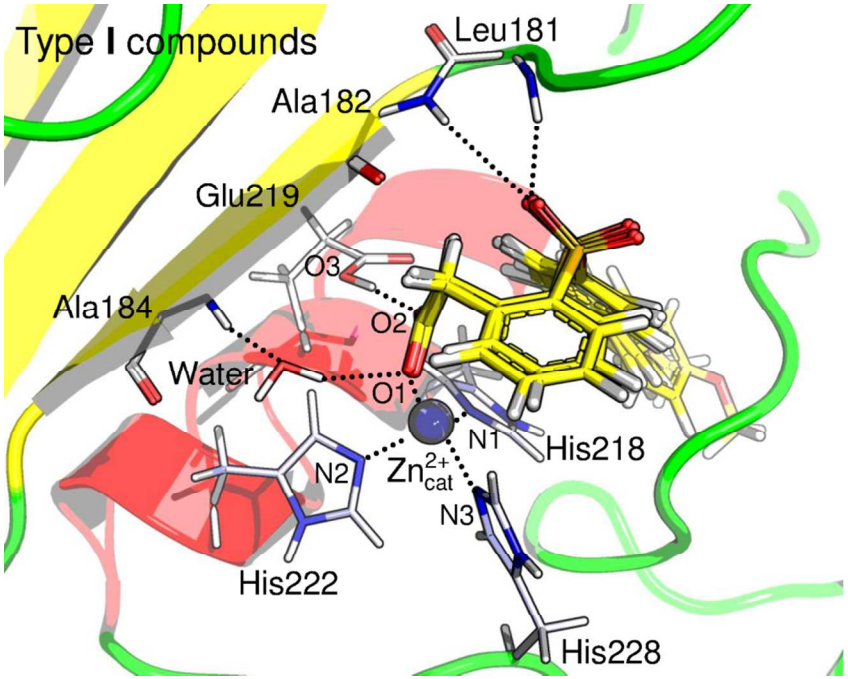

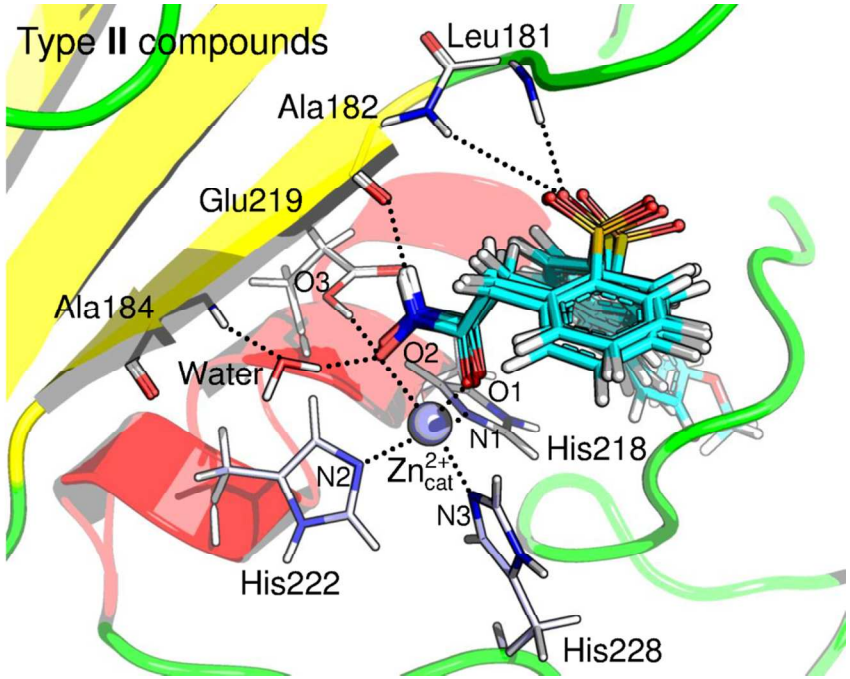

compound		distance			angle									
no.	type	d_1[a]	d_2[a]	d_3[a]	a_1[b]	a_2[b]	a_3[b]	a_4[b]	a_5[b]	a_6[b]	a_7[b]	a_8[b]	a_9[b]	a_{10}[b]
1	**I**	2.00	2.67	2.77	49.51	132.02	103.96	111.93	84.41	111.99	146.13	105.72	99.45	99.35
2	**I**	2.00	2.67	2.81	49.58	131.75	105.76	109.43	83.66	114.81	142.65	104.40	99.91	101.32
3	**I**	1.99	2.70	2.79	49.02	132.81	103.62	109.79	84.76	115.86	141.74	105.49	99.00	101.37
4	**I**	1.99	2.69	2.79	49.12	132.91	103.09	110.29	84.62	115.95	141.39	105.50	99.48	100.96
5	**II**	2.11	2.16	2.77	77.72	108.67	145.55	87.85	105.32	87.00	154.83	105.07	93.79	98.77
6	**II**	2.09	2.16	2.77	77.70	104.88	151.20	85.48	107.33	89.87	149.04	103.60	92.77	102.00
7	**II**	2.10	2.16	2.75	77.89	111.91	144.49	85.86	106.87	87.95	152.20	103.31	92.57	100.06
8	**II**	2.12	2.17	2.75	77.14	117.77	136.42	85.48	102.93	87.72	157.01	105.31	94.83	98.42

calculated structure[c,d]	**I**	2.00 (0.01)	2.68 (0.01)	2.79 (0.01)	63.46 (0.24)	121.59 (0.50)	124.26 (1.00)	98.26 (0.96)	94.99 (0.42)	101.39 (1.60)	148.12 (1.88)	104.80 (0.51)	96.48 (0.32)	100.28 (0.82)
	II	2.11 (0.01)	2.16 (0.00)	2.76 (0.01)	77.61 (0.28)	110.81 (4.73)	144.42 (5.27)	86.17 (0.98)	105.61 (1.72)	88.14 (1.06)	153.27 (2.98)	104.32 (0.88)	93.49 (0.90)	99.81 (1.40)
crystallographic structure[c,e]	**I**	1.99 (0.16)	2.71 (0.17)	2.62 (0.06)	52.29 (3.53)	118.32 (4.58)	126.29 (6.69)	96.17 (2.85)	96.71 (10.54)	91.94 (3.28)	146.18 (4.83)	101.28 (2.64)	102.92 (1.75)	109.20 (6.56)
	II	2.12 (0.16)	2.20 (0.11)	2.71 (0.19)	75.39 (3.71)	112.93 (8.97)	145.62 (10.03)	86.42 (7.95)	102.08 (8.41)	90.65 (4.72)	150.50 (7.05)	98.37 (6.31)	94.16 (3.66)	105.27 (4.88)
TH		–	–	–	–	109.47[f]	109.47[f]	109.47[f]	–	–	–	109.47[f]	109.47[f]	109.47[f]
TB		–	–	–	90[f]	120[f]	120[f]	90[f]	90[f]	90[f]	180[f]	120[f]	90[f]	90[f]
SB		–	–	–	90[f]	90[f]	180[f]	90[f]	90[f]	90[f]	180[f]	90[f]	90[f]	90[f]

[a] $d_{1–3}$ (Å) denote O1−Zn_{cat}^{2+}, O2−Zn_{cat}^{2+}, and O2−O3, respectively.

[b] $a_{1–10}$ (deg) denote O1−Zn_{cat}^{2+}−O2, O1−Zn_{cat}^{2+}−N1, O1−Zn_{cat}^{2+}−N2, O1−Zn_{cat}^{2+}−N3, O2−Zn_{cat}^{2+}−N1, O2−Zn_{cat}^{2+}−N2, O2−Zn_{cat}^{2+}−N3, N1−Zn_{cat}^{2+}−N2, N2−Zn_{cat}^{2+}−N3, and N3−Zn_{cat}^{2+}−N1, respectively.

[c] Average value and standard deviation (in parentheses).

[d] Average values of the complex structures for the types **I** and **II** compounds.

[e] Average values were obtained from the crystallographic structures of MMP-12–ligand complexes (PDB codes: 1ROS, 3EHX, 3EHY, 3TS4, 4EFS, 4H84, 4I03, and 4H30 (type **I**); 1RMZ, 1YCM, 1Z3J, 2W0D, 2W08, 2W09, 2W0A, 3F1A, 3F15, 3F16, 3F17, 3F18, 3F19, 3LK8, 3N2U, 3N2V, 3NX7, 3RTS, 3RTT, 4GUY, 1JIZ, 1JK3, 4H49, and 4H76 (type **II**)).

[f] Ideal values for tetrahedral (TH) and trigonal bipyramidal (TB)/square-based pyramid (SP) coordination spheres.

Table 3 Overall free-energy change ΔG and representative energy terms[a]

compound no.	type	ΔG_{obs}[b]	ΔG_{calc}[c]	ΔG_{calc}[d]	ΔG_{calc}[e]	$\Delta E_{bind}^{ONIOM/HF/ME}$	$\Delta E_{bind}^{ONIOM/HF/EE}$	$\Delta E_{bind}^{FMO/HF}$	ΔG_{sol}^{polar}	E_{disp}
1	**I**	−5.75	−6.41	−6.56	−6.64	−304.96	−297.71	−298.46	263.17	−61.43
2	**I**	−9.11	−9.57	−9.52	−10.09	−299.30	−290.60	−297.25	266.65	−84.58
3	**I**	−8.26	−8.12	−8.01	−7.79	−298.73	−290.04	−290.78	264.12	−76.21
4	**I**	−9.72	−8.59	−8.39	−8.52	−302.00	−292.84	−295.85	269.72	−80.62
5	**II**	−10.63	−10.29	−10.57	−10.52	−343.81	−336.40	−340.86	286.95	−63.55
6	**II**	−13.76	−13.42	−13.31	−13.77	−339.30	−329.66	−339.82	291.93	−86.90
7	**II**	−11.66	−11.78	−11.95	−11.29	−341.85	−333.70	−336.42	291.21	−76.38
8	**II**	−11.80	−12.51	−12.36	−12.07	−342.52	−332.89	−338.03	290.42	−78.15
variance (**I**)[f]						6.12	9.15	8.56	6.44[g]	76.76
variance (**II**)[f]						2.70	5.78	2.90	3.65[g]	69.62
variance (**I** + **II**)[f]						416.93	414.84	472.22	151.61[g]	73.26

[a] In kcal/mol.

[b] $\Delta G_{obs} = RT \ln IC_{50}$ (T = 310 K).

[c] Calculated from eq 1.

[d] Calculated from eq 2.

[e] Calculated from eq 3.

[f] In kcal^2/mol^2.

[g] The corresponding variances (**I**), (**II**), and (**I** + **II**) of $\Delta G_{sol}^{nonpolar}$ are 0.28, 0.28, and 0.29 kcal^2/mol^2, respectively, implying that the contribution of $\Delta G_{sol}^{nonpolar}$ is negligible.

Figure captions

Fig. 1 Schematic representation of the interaction of the arylsulfone inhibitor (compound **6**) with amino acid residues in the active site of MMP-12. Atoms described here except for those in the zinc binding group were optimized in the ONIOM calculations. Atoms in QM region are colored blue. Dotted lines indicate hydrogen and coordination bonds.

Fig. 2 Plots of ΔG_{obs} with (a) Clog *P* (classical QSAR), (b) CDOCKER energy (docking), and (c) ΔG_{calc} (LERE-QSAR). Solid and open circles represent the types **I** and **II** compounds, respectively.

Fig. 3 Variations in the representative energy terms. $\Delta E_{bind}^{ONIOM/HF/ME}$, E_{disp}, and ΔG_{sol}^{polar} are relative energies from those of compound **1**. ΔG_{calc} is calculated by eq 1.

Fig. 4 Interaction profiles of IFIED between arylsulfone inhibitors and amino acid residues in MMP-12. (a) IFIED values of compounds **2** and **6** with residues. (b) Variances of IFIED values among the total eight compounds as well as among each type of compound. Some large peaks are represented by circle.

Fig. 5 (a) IFIED values of compounds **1**–**8** with Ala182, the water molecule, Ca_{III}^{2+}, Zn_{str}^{2+}, and Zn_{cat}^{2+} blocks. (b) The binding modes of the carboxylic and hydroxamic acid zinc binding groups

in compounds **2** and **6** (stick model with yellow and cyan, respectively) to the catalytic zinc binding site of MMP-12.

Fig. 6 (a) IFIED values of compounds **1**–**8** with Leu214, Thr215, Val235, Met236, Tyr240, and Lys241. (b) The binding modes of the aryl substituents in the type **II** compounds (stick model with cyan) to the hydrophobic pocket of MMP-12.

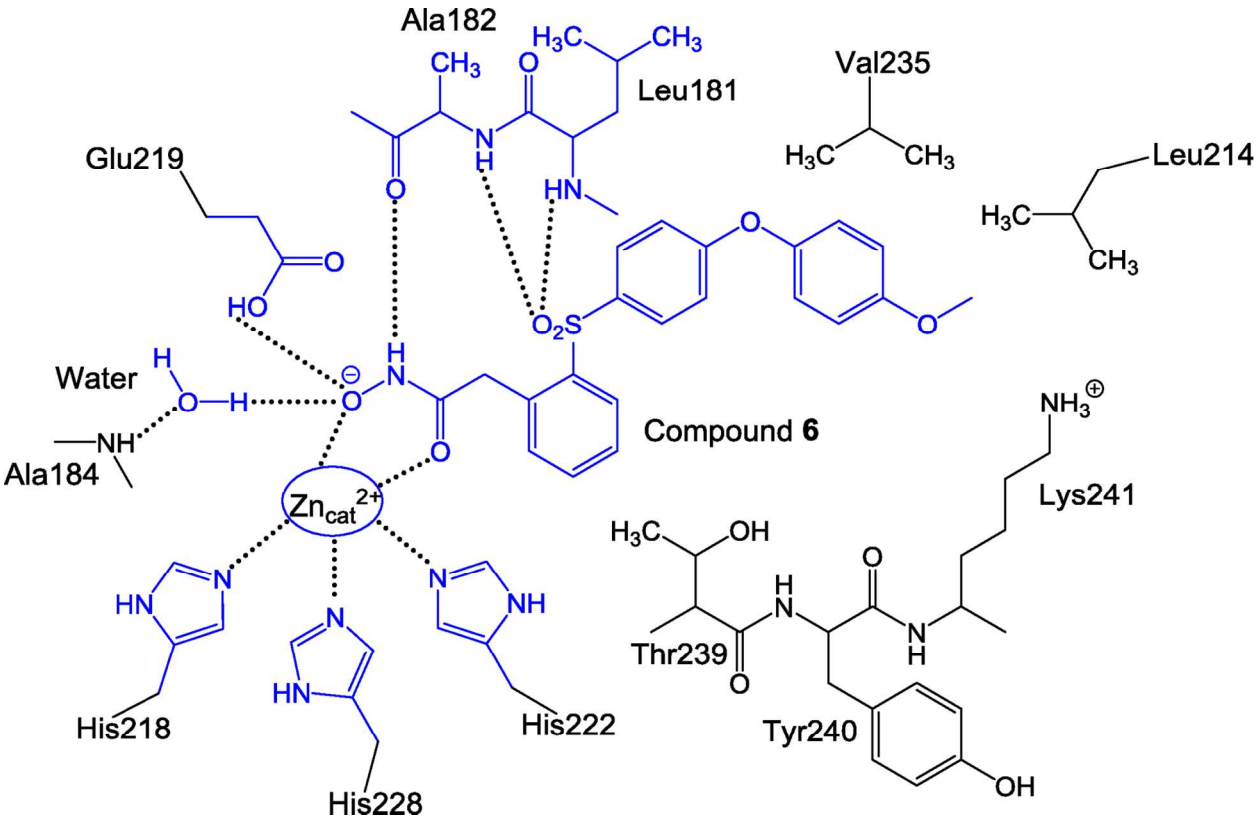

Fig. 1 Schematic representation of the interaction of the arylsulfone inhibitor (compound **6**) with amino acid residues in the active site of MMP-12. Atoms described here except for those in the zinc binding group were optimized in the ONIOM calculations. Atoms in QM region are colored blue. Dotted lines indicate hydrogen and coordination bonds.

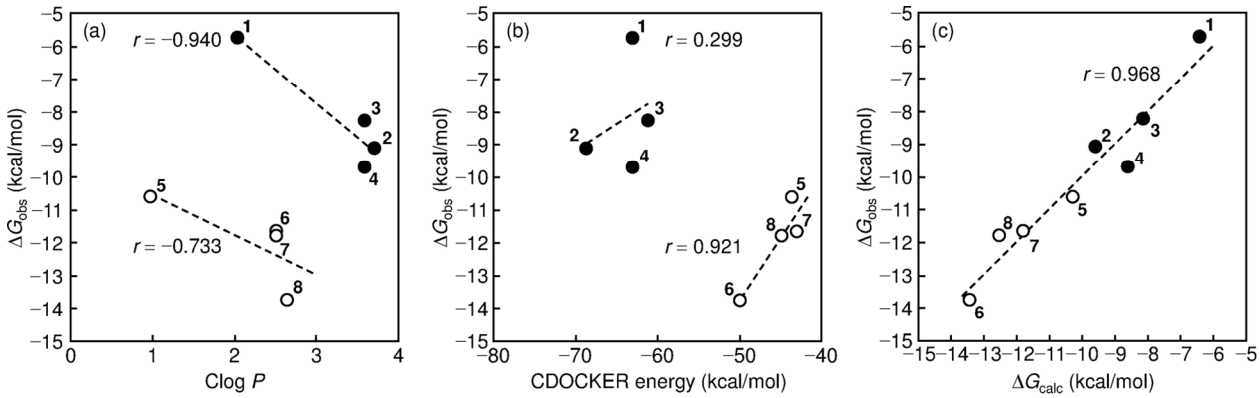

Fig. 2 Plots of ΔG_{obs} with (a) Clog *P* (classical QSAR), (b) CDOCKER energy (docking), and (c) ΔG_{calc} (LERE-QSAR). Solid and open circles represent the types **I** and **II** compounds, respectively.

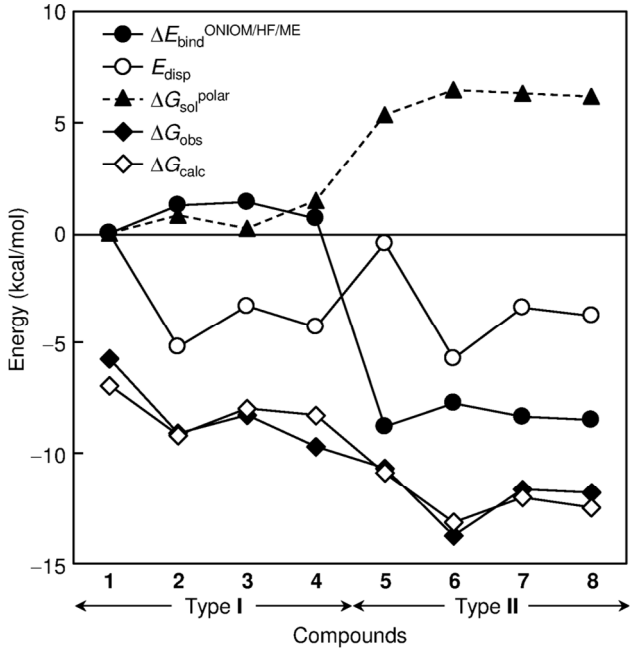

Fig. 3 Variations in the representative energy terms. $\Delta E_{bind}^{ONIOM/HF/ME}$, E_{disp}, and ΔG_{sol}^{polar} are relative energies from those of compound **1**. ΔG_{calc} is calculated by eq 1.

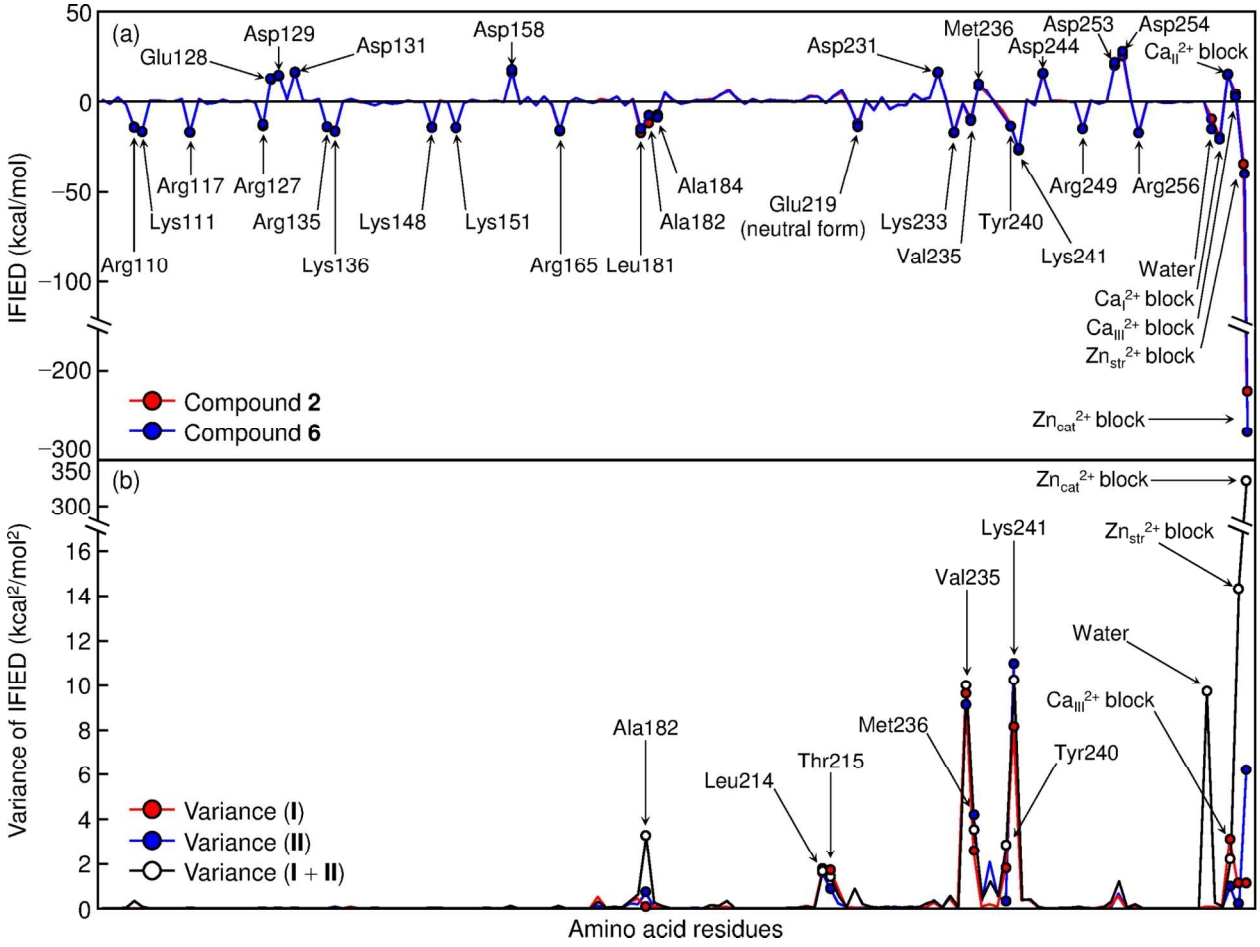

Fig. 4 Interaction profiles of IFIED between arylsulfone inhibitors and amino acid residues in MMP-12. (a) IFIED values of compounds **2** and **6** with residues. (b) Variances of IFIED values among the total eight compounds as well as among each type of compound. Some large peaks are represented by circle.

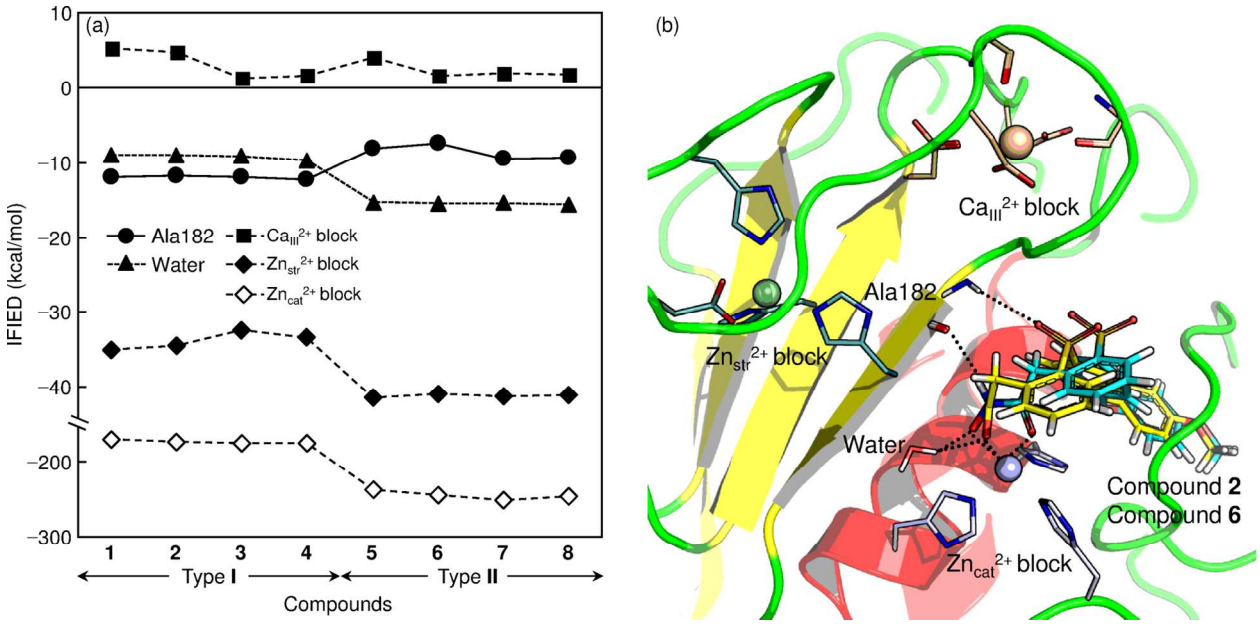

Fig. 5 (a) IFIED values of compounds **1**–**8** with Ala182, the water molecule, Ca_{III}^{2+}, Zn_{str}^{2+}, and Zn_{cat}^{2+} blocks. (b) The binding modes of the carboxylic and hydroxamic acid zinc binding groups in compounds **2** and **6** (stick model with yellow and cyan, respectively) to the catalytic zinc binding site of MMP-12.

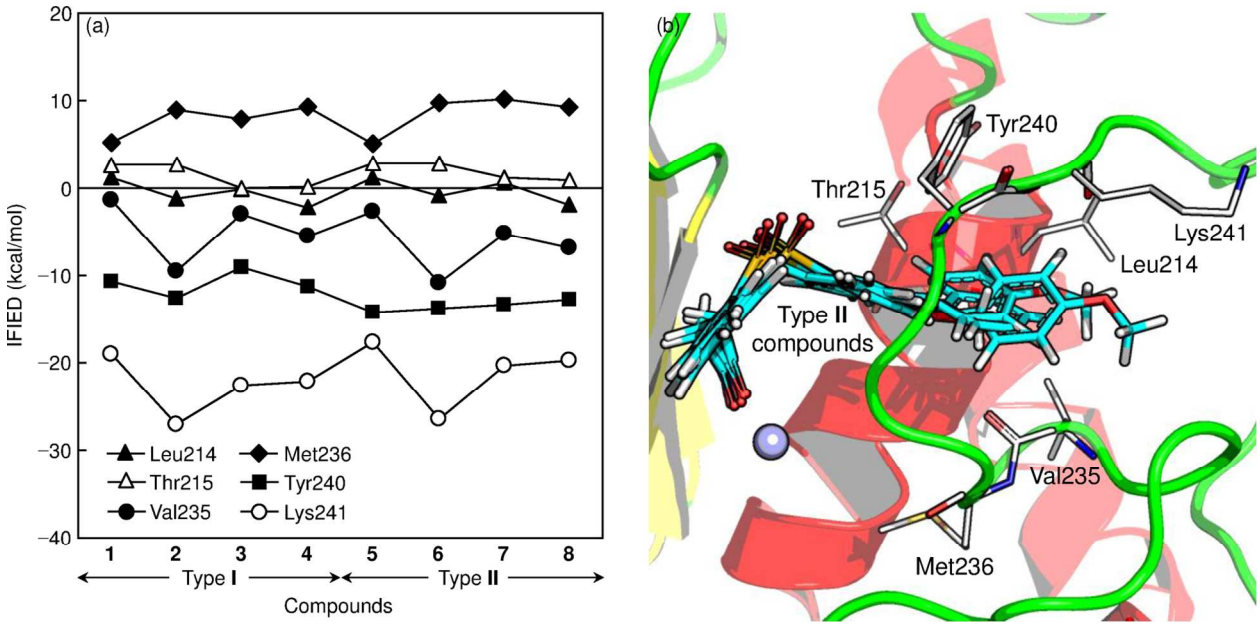

Fig. 6 (a) IFIED values of compounds **1**–**8** with Leu214, Thr215, Val235, Met236, Tyr240, and Lys241. (b) The binding modes of the aryl substituents in the type **II** compounds (stick model with cyan) to the hydrophobic pocket of MMP-12.